Article

Experimental Determination of the QCD Effective Charge $\alpha_{g_1}(Q)$

Alexandre Deur [1,2,*], Volker Burkert [1], Jian-Ping Chen [1] and Wolfgang Korsch [3]

1   Thomas Jefferson National Accelerator Facility, Physics Division, Newport News, VA 23606, USA; burkert@jlab.org (V.B.); jpchen@jlab.org (J.-P.C.)
2   Department of Physics, University of Virginia, Charlottesville, VA 22904, USA
3   Department of Physics & Astronomy, University of Kentucky, Lexington, KY 40506, USA; wkkors0@g.uky.edu
*   Correspondence: deurpam@jlab.org

Abstract: The QCD effective charge $\alpha_{g_1}(Q)$ is an observable that characterizes the magnitude of the strong interaction. At high momentum Q, it coincides with the QCD running coupling $\alpha_s(Q)$. At low Q, it offers a nonperturbative definition of the running coupling. We have extracted $\alpha_{g_1}(Q)$ from measurements carried out at Jefferson Lab that span the very low to moderately high Q domain, $0.14 \leq Q \leq 2.18$ GeV. The precision of the new results is much improved over the previous extractions and the reach in Q at the lower end is significantly expanded. The data show that $\alpha_{g_1}(Q)$ becomes Q-independent at very low Q. They compare well with two recent predictions of the QCD effective charge based on Dyson–Schwinger equations and on the AdS/CFT duality.

1. Introduction

The behavior of quantum chromodynamics (QCD), the gauge theory of the strong interaction, is determined by the magnitude of its coupling α_s. It is large at low momentum, characterized here by $Q \equiv \sqrt{-q^2}$ with q^2 the square of momentum transferred in the process of electromagnetically probing a hadron. For $Q \ll 1$ GeV, $\alpha_s(Q) \gtrsim 1$, which is one of the crucial pieces leading to quark confinement. For $Q \gg 1$ GeV, $\alpha_s(Q) \lesssim 0.2$, which enables the use of perturbative computational techniques (perturbative QCD, pQCD) constituting an accurate analytical approximation of QCD. In this domain, α_s^{pQCD} is well defined and known within an accuracy of 1% at $Q = M_{Z^0} = 91$ GeV, the Z^0 mass, and within a few percents at Q values of a few GeV [1]. However, using pQCD at $Q \lesssim 1$ GeV produces a diverging α_s^{pQCD} (Landau pole) that prohibits any perturbative expansion in α_s^{pQCD} and signals the breakdown of pQCD. In contrast, most nonperturbative methods, including lattice QCD [2], the AdS/CFT (Anti-de-Sitter/Conformal Field Theory) duality [3,4] implemented using QCD's light-front (LF) quantization [5] and a soft-wall AdS potential (Holographic LF QCD, HLFQCD [6]) or solving the Dyson–Schwinger equations (DSEs) [7] yield a finite α_s. In fact, many theoretical approaches predict that α_s "freezes" as $Q \to 0$, viz, it loses its Q-dependence [8].

There are several possible definitions of α_s in the nonperturbative domain ($Q \lesssim 1$ GeV) [8]. We use here the *effective charge* approach that defines α_s from the perturbative series of an observable truncated to its first order in α_s [9]. Although this definition can be applied for any Q value, it was initially proposed for the pQCD domain where it makes α_s the equivalent of the Gell-Mann Low coupling of quantum electrodynamics (QED), α [10]. With this definition, α_s can be evaluated at any Q value, has no low Q divergence and is analytic around quark mass thresholds. Furthermore, since the first order in α_s^{pQCD} of a pQCD approximant is independent of the choice of renormalization scheme

(RS), effective charges are independent of RS and gauge choices. This promotes α_s from a parameter depending on chosen conventions to an observable, albeit with the caveat that it becomes process-dependent since two observables produce generally different effective charges. Yet, pQCD predictability is maintained because effective charges are related without renormalization scale ambiguities by commensurate scale relations (CSR) [11]. CSR are known to hold for pQCD and QED since the latter corresponds to the $N_C \to 0$ limit of QCD, with N_C the number of colors. For example, CSR explicitly relate α_{g_1}, α_{F_3}, α_τ and α_R defined using the generalized Bjorken sum rule [12], the Gross–Llewellyn Smith sum rule [13], and the perturbative approximant for the τ-decay rate [14] and $R_{e^+e^-}$ [15], respectively. In fact, the choice of process to define an effective charge is analogous to an RS choice for α_s^{pQCD} [16] and the procedure of extracting an effective charge, e.g., from τ-decay the τ-scheme is denoted. Here, we discuss the effective charge $\alpha_{g_1}(Q)$ (g_1-scheme) extracted using the generalized Bjorken sum rule:

$$
\begin{aligned}
\Gamma_1^{\text{p}-\text{n}}(Q^2) &\equiv \int_0^{1^-} g_1^{\text{p}}(x, Q^2) - g_1^{\text{n}}(x, Q^2) dx = \frac{g_A}{6}\left[1 - \frac{\alpha_s^{\text{pQCD}}(Q)}{\pi} - 3.58\left(\frac{\alpha_s^{\text{pQCD}}(Q)}{\pi}\right)^2 \right. \\
&\left. -20.21\left(\frac{\alpha_s^{\text{pQCD}}(Q)}{\pi}\right)^3 - 175.7\left(\frac{\alpha_s^{\text{pQCD}}(Q)}{\pi}\right)^4 + \mathcal{O}\left((\alpha_s^{\text{pQCD}})^5\right)...\right] + \textstyle\sum_{n>1} \frac{\mu_{2n}}{Q^{2n-2}},
\end{aligned}
\tag{1}
$$

where x is the Bjorken scaling variable [17], $g_A = 1.2762(5)$ [2] is the nucleon axial charge, $g_1^{\text{p(n)}}$ is the longitudinal spin structure function of the proton (neutron) obtained in polarized lepton-nucleon scattering [18] and μ_{2n} are the operator product expansion's (OPE) nonperturbative higher twist (HT) terms. The integral excludes the elastic contribution at $x = 1$. The series coefficients are computed for $n_f = 3$ and in the $\overline{\text{MS}}$ RS for the $n > 1$ α_s^n terms [19]. They originate from the pQCD radiative corrections. Although the expansion (1) is only applicable in the perturbative domain, i.e., at distance scales where confinement effects are weak, the HT terms can be related to the latter [20], and one may picture the terms of Equation (1) as coherently merging together at low Q to produce confinement.

The effective charge α_{g_1} is defined from Equation (1) expressed at first order in coupling and twist:

$$
\Gamma_1^{\text{p}-\text{n}}(Q^2) \equiv \frac{g_A}{6}\left(1 - \frac{\alpha_{g_1}(Q)}{\pi}\right) \longrightarrow \alpha_{g_1}(Q) \equiv \pi\left(1 - \frac{6}{g_A}\Gamma_1^{\text{p}-\text{n}}(Q)\right).
\tag{2}
$$

Thus, in the domain where Equation (2) applies, α_{g_1} can be interpreted as a running coupling that not only includes short-distance effects such as vertex correction and vacuum polarization, but all other effects, e.g., pQCD radiative corrections and, in the lower-Q domain of pQCD, HT terms and other nonperturbative effects not formalized by OPE and therefore not included in Equation (2). The latter comes from coherent reactions of a hadron (resonances). In the nonperturbative domain where pQCD radiative corrections and HT effects have merged into global confinement effects, α_{g_1} may approximately retain its interpretation as a coupling if the contribution to $\Gamma_1^{\text{p}-\text{n}}$ of nonresonant reactions continues to dominate, as they do at large Q [21].

There are several advantages to α_{g_1} [8]. First, rigorous sum rules constrain $\alpha_{g_1}(Q)$ for $Q \to 0$ (the Gerasimov–Drell–Hearn (GDH) sum rule [22]) and $Q \to \infty$ (the Bjorken sum rule). They provide analytical expressions of $\alpha_{g_1}(Q)$ in these limits (blue dashed line and cyan hatched band in Figure 1). Furthermore, contributions from Δ baryons are quenched in $\Gamma_1^{\text{p}-\text{n}}$ [23], enhancing the nonresonant reactions contribution to $\Gamma_1^{\text{p}-\text{n}}$ relatively to the resonance contribution, which helps toward interpreting α_{g_1} as a coupling. If so, α_{g_1} would remain approximately equivalent to the Gell-Mann Low coupling in the nonperturbative domain, a crucial property that it is not obvious and may be specific to α_{g_1}. Such a property is supported by the agreement between α_{g_1} and calculations of couplings [24,25] using a definition consistent with α_{g_1}.

Former extractions of α_{g_1} [26] were obtained from experimental data on Γ_1^{p-n} from CERN [27], DESY [28], Jefferson Lab (JLab) [29] and SLAC [30]; see Figure 1. Since the results reported in Ref. [26], progress has occurred on both the experimental and theoretical fronts. Firstly, when Ref. [26] was published, the meaning of α_{g_1} in the nonperturbative region was unclear. Thus, the comparison in [26] of α_{g_1} to theoretical predictions of the nonperturbative coupling was tentative. This is now better understood: as just discussed, α_{g_1} essentially retains its meaning of effective charge at low Q [8,21]. Secondly, new data on Γ_1^{p-n} have become available from CERN (COMPASS experiment) [31] and JLab (EG1dvcs experiment) [32] at high Q, and from JLab (E97110, E03006 and E05111 experiments) [33] at very low Q. Finally, new theoretical studies of the nonperturbative behavior of α_s were conducted, including the first use of the AdS/CFT duality to describe the strong coupling in its nonperturbative domain [24] and the identification of a process-independent (PI) effective charge $\hat{\alpha}_{PI}(Q)$ that unifies a large body of research from DSE and lattice QCD to α_s [25,34]. Connections between the nonperturbative and perturbative effective charges were made [8,16,35], which permitted a prediction of α_s at the Z_0 pole, $\alpha_s^{\overline{MS}}(M_z^2) = 0.1190 \pm 0.0006$ at N³LO [36] that agrees well with the 2021 Particle Data Group compilation, $\alpha_s(M_Z) = 0.1179 \pm 0.0009$ [2]. In addition to predicting quantities characterizing hadronic structures [3,25,37], the effective charge helps establish conformal behavior at low Q. Through AdS/CFT, this helps the investigation of the physics beyond the standard model [4] or of the quark-gluon plasma [38] in heavy ion collisions [39] and nuclear hydrodynamics [40] for the latter and neutron stars [41].

Here, we report on new experimental data on α_{g_1} extracted from [31–33] and how they compare with the latest theory predictions.

2. Experimental Extraction of α_{g_1}

The new JLab data on $\Gamma_1^{p-n}(Q)$ were taken by four experiments. The first experiment, E97110 [42], occurred in Hall A [43] of JLab. The three others used the CLAS spectrometer [44] in JLab's Hall B and were experiments EG1dvcs [45], E03006 [46] and E05111 [47] (the two latter being referred to as Experimental Group EG4). The four experiments occurred during the 6 GeV era of JLab, before its 12 GeV upgrade. The experiments used a polarized electron beam with energies ranging from 0.8 to 6 GeV. E97110 studied the spin structures of the neutron and ³He using the Hall A polarized ³He target with longitudinal and transverse polarization directions [48]. EG1dvcs, E03006, and E05111 studied the proton, neutron and deuteron spin structures using the Hall B longitudinally polarized ammonia (NH_3 or ND_3) target [49]. The main purpose of EG1dvcs was high Q, up to 2.65 GeV ($Q^2 = 7$ GeV²), exclusive measurements of deep virtual Compton scattering. Therefore, it provided highly precise inclusive Γ_1^{p-n} data compared to the older data in the same domain [27–30]. E97110, E03006 and E05111 were dedicated to test chiral effective field theory predictions by covering very low Q domains: $0.19 \le Q \le 0.49$, $0.11 \le Q \le 0.92$ and $0.14 \le Q \le 0.70$ GeV, respectively. To reach low Q while covering the large x range necessary for the Γ_1 integral, high beam energy (up to 4.4 GeV) was needed, and the scattered electrons had to be detected at small angles (down to about 5°). In Hall A, the low angles were reached via a supplementary dipole magnet installed in front of the spectrometer [50]. In Hall B, a Cherenkov counter designed for high efficiency at small angles was installed in one of the six sectors of CLAS [47] for which magnetic field was set to bent outward the scattered electrons. In addition, both the Hall A and B targets were placed about 1 m upstream of their usual positions.

The EG1dvcs data on protons and deuterons were combined to form Γ_1^{p-n} over the range $0.78 \le Q \le 2.18$ GeV [32]. The Γ_1^{p-n} formed with the E97110 and EG4 data covers the $0.14 \le Q \le 0.70$ GeV range [33]. The α_{g_1} data, obtained following Equation (2), are shown in Figure 1 and given in Table 1. Also shown in the figure are the older data presented in Ref. [29], including α_{F_3} extracted from the data [51] and $\alpha_{g_1(\tau)}$ from the OPAL data on τ-decay [14]. The effective charge α_{F_3} is nearly identical to α_{g_1} [26], and $\alpha_{g_1(\tau)}$ was

transformed from the τ-scheme to the g_1-scheme using the CSR [11]. Consequently, α_{F_3} and $\alpha_{g_1(\tau)}$ are directly comparable to α_{g_1}. We also show in Figure 1 the theory predictions from AdS/CFT [24] and DSE [25]. Remarkably, both predictions are parameter-free and gauge-invariant.

Table 1. Data on $\alpha_{g_1}(Q)$ from JLab experiments EG4 (top, from $Q = 0.143$ GeV to 0.704 GeV), EG4/E97110 (middle, from $Q = 0.187$ GeV to 0.490 GeV) and EG1dvcs (bottom, from $Q = 0.775$ GeV to 2.177 GeV).

Q (GeV)	$\alpha_{g_1} \pm$ stat. $\pm$ syst.
0.143	$3.064 \pm 0.043 \pm 0.018$
0.156	$3.129 \pm 0.046 \pm 0.019$
0.171	$2.955 \pm 0.046 \pm 0.023$
0.187	$3.083 \pm 0.044 \pm 0.024$
0.204	$3.022 \pm 0.049 \pm 0.024$
0.223	$3.002 \pm 0.052 \pm 0.027$
0.243	$2.988 \pm 0.055 \pm 0.031$
0.266	$2.947 \pm 0.060 \pm 0.035$
0.291	$2.983 \pm 0.065 \pm 0.035$
Q (GeV)	$\alpha_{g_1} \pm$ stat. $\pm$ syst.
0.317	$2.961 \pm 0.062 \pm 0.038$
0.347	$2.730 \pm 0.070 \pm 0.044$
0.379	$2.853 \pm 0.077 \pm 0.040$
0.414	$2.745 \pm 0.076 \pm 0.041$
0.452	$2.779 \pm 0.090 \pm 0.043$
0.494	$2.451 \pm 0.094 \pm 0.044$
0.540	$2.397 \pm 0.092 \pm 0.039$
0.590	$2.349 \pm 0.101 \pm 0.040$
0.645	$2.431 \pm 0.109 \pm 0.043$
0.704	$1.996 \pm 0.131 \pm 0.104$
Q (GeV)	$\alpha_{g_1} \pm$ stat. $\pm$ syst.
0.187	$3.016 \pm 0.009 \pm 0.027$
0.239	$2.973 \pm 0.015 \pm 0.035$
0.281	$2.952 \pm 0.021 \pm 0.041$
0.316	$2.929 \pm 0.017 \pm 0.048$
0.387	$2.815 \pm 0.021 \pm 0.076$
0.447	$2.704 \pm 0.025 \pm 0.086$
0.490	$2.575 \pm 0.031 \pm 0.053$
0.775	$1.743 \pm 0.007 \pm 0.071$
0.835	$1.571 \pm 0.007 \pm 0.101$
0.917	$1.419 \pm 0.009 \pm 0.132$
0.986	$1.341 \pm 0.010 \pm 0.147$
1.088	$1.272 \pm 0.010 \pm 0.156$
1.167	$1.121 \pm 0.013 \pm 0.153$
1.261	$0.955 \pm 0.016 \pm 0.146$
1.384	$0.874 \pm 0.016 \pm 0.269$
1.522	$0.730 \pm 0.012 \pm 0.280$
1.645	$0.708 \pm 0.009 \pm 0.257$
1.795	$0.617 \pm 0.007 \pm 0.254$
1.967	$0.581 \pm 0.006 \pm 0.223$
2.177	$0.636 \pm 0.003 \pm 0.187$

The AdS/CFT coupling $\alpha_{g_1}^{\mathrm{HLF}}$ is obtained in the HLFQCD approach where QCD is quantized using LF coordinates [5]. The use of the HLFQCD approach incorporates the underlying conformal (i.e., scale-invariant) character of QCD at low and large Q. The deformation of the AdS_5 space is dual to a semiclassical potential that models quark confinement. This potential can be determined with various methods that all lead to the same harmonic oscillator form [3,52,53]. The effective charge $\alpha_{g_1}^{\mathrm{HLF}}$ is dual to the product of the AdS_5 coupling *constant* by the AdS_5 space deformation term. Since the latter is dual to the CFT confinement force, the meaning of $\alpha_{g_1}^{\mathrm{HLF}}$ is analogous to that of α_{g_1}, which, at low Q, incorporates in α_s confinement effects. The Q-dependence of $\alpha_{g_1}^{\mathrm{HLF}}$ is controlled by a single scale, e.g., the proton mass. The coupling is normalized to $\alpha_{g_1}^{\mathrm{HLF}}(0) = \pi$ to obey the kinematic constraint that $\Gamma_1^{\mathrm{p-n}}(0) = 0$, i.e., $\alpha_{g_1}(0) = \pi$, see Equation (2). This normalization amounts to the RS choice of pQCD [16]. Thus, the $\alpha_{g_1}^{\mathrm{HLF}}(Q)$ prediction is parameter-free. Above $Q \simeq 1$ GeV, HLFQCD ceases to be valid because its *semiclassical* potential does not include, by definition, the short distance quantum effects responsible for the running of a coupling. This is palliated by matching HLFQCD and pQCD near $Q \simeq 1$ GeV where both formalisms apply, thereby providing $\alpha_{g_1}^{\mathrm{HLF}}(Q)$ at all Q [16].

The DSE effective charge $\hat{\alpha}_{\mathrm{PI}}$ [25] is obtained starting with the pinch technique [54] and background field method [55]. They allow us to define a process-independent QCD coupling in terms of a mathematically reconstructed gluon two-point function analogous to the Gell-Mann Low effective charge of QED. The $\hat{\alpha}_{\mathrm{PI}}$ is then computed by combining the solution of DSE compatible with lattice QCD results. The definition of $\hat{\alpha}_{\mathrm{PI}}$ explicitly factors in a renormalization group invariant interaction, thus causing it, like $\alpha_{g_1}(Q)$ and $\alpha_{g_1}^{\mathrm{HLF}}(Q)$, to incorporate confinement [56]. Like them, $\hat{\alpha}_{\mathrm{PI}}(Q)$ freezes at low Q with a predicted infrared fixed-point of $\hat{\alpha}_{\mathrm{PI}}(0) = (0.97 \pm 0.04)\pi$. The mechanism at the origin of the freezing in the DSE framework is the emergence of a dynamical gluon mass $m_g(Q)$ [54,57] that (A) regulates the Landau pole and (B) decouples the dynamics at scales $Q \lesssim m_g(0)$, thereby causing the coupling to lose its Q-dependence [58]. Like $\alpha_{g_1}^{\mathrm{HLF}}$, $\hat{\alpha}_{\mathrm{PI}}$ is parameter-free and gauge-invariant but, in contrast to the former and α_{g_1}, $\hat{\alpha}_{\mathrm{PI}}$ is also process-independent. No parameter is varied to predict the infrared fixed-point $\hat{\alpha}_{\mathrm{PI}}(0)$ since it is largely fixed by the value of $m_g(0)$, nor is a matching necessary to ensure agreement with the perturbative determination of $\alpha_{g_1}^{\mathrm{pQCD}}$ from the renormalization group equations and the Bjorken sum rule. Crucially, the practical determination of $\hat{\alpha}_{\mathrm{PI}}(Q)$ consistently incorporates the extensive information from Lattice QCD on the gluon and ghost propagators, thereby connecting this technique to α_{g_1}.

The new data on α_{g_1} agree well with the older data and display a much improved precision over the whole Q range covered. In addition, the data now reach clearly the freezing domain of QCD at very low Q. That α_{g_1} freezes could be already inferred with the old data but only by complementing them with the GDH sum rule or/and the $\alpha_{g_1}(0) = \pi$ constraint. For the first time, the onset of freezing is now visible with data only. One notes that only three of the lowest Q points agree with the GDH expectation. This may signal a fast arising Q-dependence beyond the leading behavior given by GDH. The data agree well with the $\alpha_{g_1}^{\mathrm{HLF}}$ and $\hat{\alpha}_{\mathrm{PI}}$ predictions. That such agreements would occur was not obvious and is a significant finding. The possible tension between the data and $\hat{\alpha}_{\mathrm{PI}}$ for the range $0.3 \lesssim Q \lesssim 0.5$ GeV may be because α_{g_1} and $\hat{\alpha}_{\mathrm{PI}}$ are not exactly the same effective charges (e.g., at high Q, $\alpha_{g_1}/\hat{\alpha}_{\mathrm{PI}} \simeq 1 + 0.05\alpha_s^{\mathrm{pQCD}} \neq 1$), but it is noteworthy that it occurs only in the moderately low Q domain where the ghost-gluon vacuum effect as computed in the Landau gauge contributes the most to $\hat{\alpha}_{\mathrm{PI}}$.
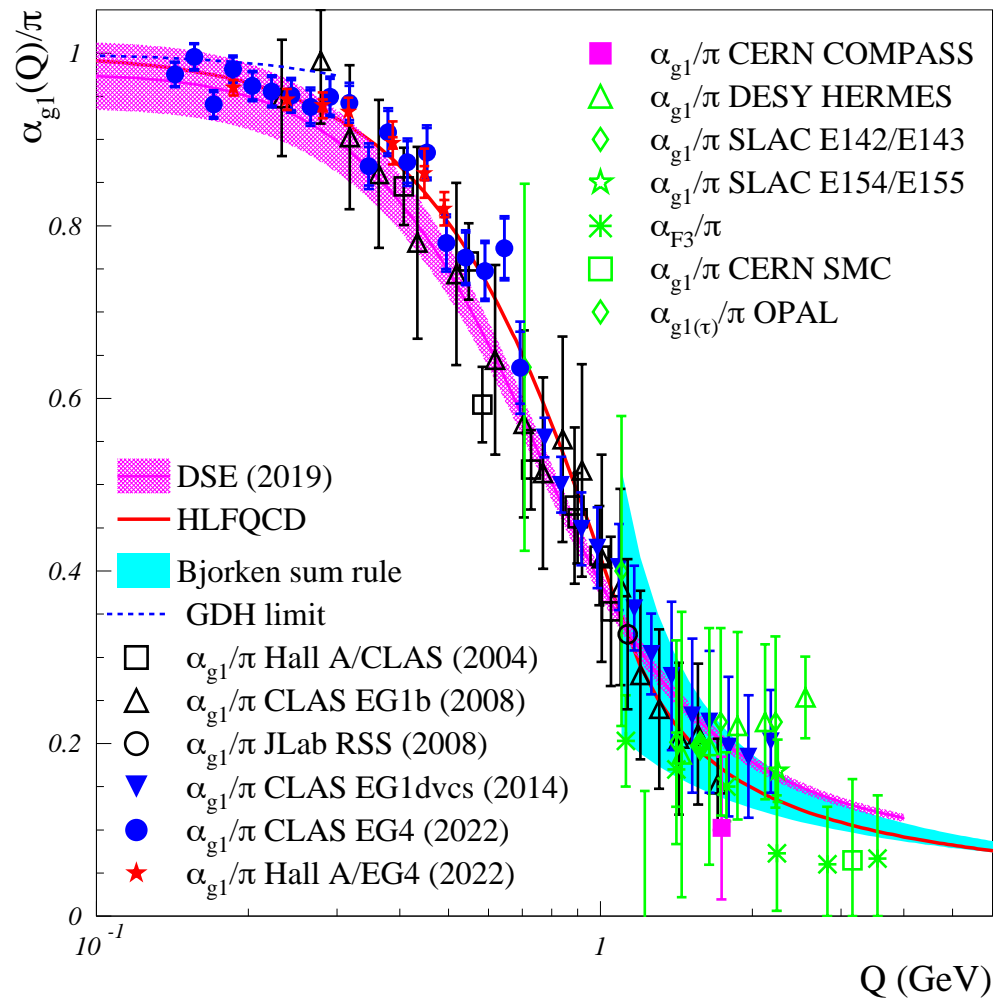
Figure 1. Effective charge $\alpha_{g_1}(Q)/\pi$ obtained from JLab experiments E03006/E97110 [33] (solid stars), E03006/E05111 [33] (solid circles) and EG1dvcs [32] (solid triangles) and from COMPASS [31] (solid square). Inner error bars represent the statistical uncertainties, and outer ones represent the systematic and statistical uncertainties added quadratically. The open symbols show the older world data [27–30] with the error bars the quadratic sum of the systematic and statistical uncertainties. Also shown are the HLFQCD [24] (red line, using the HLFQCD scale $\kappa = 0.534$ GeV [59]) and DSE [25] (magenta line and hatched band) parameter-free predictions of effective charges. The dashed line and hatched cyan band are $\alpha_{g_1}(Q)/\pi$ obtained from the GDH and Bjorken sum rules, respectively.

3. Summary and Conclusions

We used the new JLab data and COMPASS datum on the Bjorken sum to extract the QCD effective charge $\alpha_{g_1}(Q)$ in the Q-range $0.14 \leq Q \leq 2.18$ GeV. The new result displays a significantly higher precision compared to the older extractions of $\alpha_{g_1}(Q)$, and improve the low Q reach by about a factor of 2.

The new data show that $\alpha_{g_1}(Q)$ "freezes", viz, loses its Q-dependence, at small Q, saturating at an infrared fixed-point $\alpha_{g_1}(Q \simeq 0) \simeq \pi$. This was already apparent with the older data when combined with the GDH sum rule expectation, but the new data explicitly display the behavior without needing the sum rule and with significantly higher precision. The freezing of $\alpha_{g_1}(Q)$ together with the smallness of the light quark masses makes QCD approximately conformal at low Q. The conformal behavior vanishes when transiting from the low-Q effective degrees of freedom of QCD (hadrons) to the large-Q fundamental ones (partons) where conformality is then restored (the long-known Bjorken scaling [17]). This transition is revealed by the drastic change of value of the effective charge. It occurs at a Q value indicative of the chiral symmetry breaking parameter, $\Lambda_B \simeq 1$ GeV. The breaking at

low *Q* of chiral symmetry, one of the crucial properties of QCD, is believed to cause the emergence of the global properties of hadrons.

The new data agree well with sum rule predictions and with the latest predictions from DSE and from a AdS/CFT-based approach. They show that a strong coupling can be consistently defined in the nonperturbative domain of QCD, namely as an effective charge analogous to the definition used in QED, and that it can then be used to compute a large variety of hadronic quantities and other phenomena in which the strong interaction plays a role.

References

1. D'Enterria, D.; Kluth, S.; Zanderighi, G.; Ayala, C.; Benitez-Rathgeb, M.A.; Bluemlein, J.; Xie, K. The strong coupling constant: State of the art and the decade ahead. *arXiv* **2022**, arXiv:2203.08271.
2. Yao, W.M.; Amsler, C.; Asner, D.; Barnett, R.M.; Beringer, J.; Burchat, P.R.; Staney, T. Review of Particle Physics. *J. Phys. G Nucl. Part. Phys.* **2006**, *33*, 1–1232. [CrossRef]
3. Brodsky, S.J.; de Téramond, G.F.; Dosch, H.G.; Erlich, J. Light-front holographic QCD and emerging confinement. *Phys. Rep.* **2015**, *584*, 1–105. [CrossRef]
4. Dobado, A.; Espriu, D. Strongly coupled theories beyond the Standard Model. *Prog. Part. Nucl. Phys.* **2020**, *115*, 103813. [CrossRef]
5. Dirac, P.A.M. Forms of relativistic dynamics. *Rev. Mod. Phys.* **1949**, *21*, 392. [CrossRef]
6. Brodsky, S.J.; de Téramond, G.F. Light-front hadron dynamics and AdS/CFT correspondence. *Phys. Lett. B* **2004**, *582*, 211–221. [CrossRef]
7. Maris, P.; Roberts, C.D. Dyson-Schwinger equations: A Tool for hadron physics. *Int. J. Mod. Phys. E* **2003**, *12*, 297–365. [CrossRef]
8. Deur, A.; Brodsky, S.J.; de Téramond, G.F. The QCD Running Coupling. *Prog. Part. Nucl. Phys.* **2016**, *90*, 1. [CrossRef]
9. Grunberg, G. Renormalization Group Improved Perturbative QCD. *Phys. Lett.* **1980**, *95B*, 70; Erratum in *Phys. Lett.* **1982**, *110B*, 501. [CrossRef]
10. Gell-Mann, M.; Low, F.E. Quantum electrodynamics at small distances. *Phys. Rev.* **1954**, *95*, 1300. [CrossRef]
11. Brodsky, S.J.; Lu, H.J. Commensurate scale relations in quantum chromodynamics. *Phys. Rev. D* **1995**, *51*, 3652. [CrossRef] [PubMed]
12. Bjorken, J.D. Applications of the Chiral $U(6) \times U(6)$ Algebra of Current Densities. *Phys. Rev.* **1966**, *148*, 1467. [CrossRef]
13. Gross, D.J.; Smith, C.H.L. High-energy neutrino-nucleon scattering, current algebra and partons. *Nucl. Phys. B* **1969**, *14*, 337. [CrossRef]
14. Brodsky, S.J.; Menke, S.; Merino, C.; Rathsman, J. On the behavior of the effective QCD coupling alpha(tau)(s) at low scales. *Phys. Rev. D* **2003**, *67*, 055008. [CrossRef]
15. Gorishnii, S.G.; Kataev, A.L.; Larin, S.A. The $O(\alpha_s^3)$-corrections to $\sigma_{tot}(e^+e^- \rightarrow hadrons)$ and $\Gamma(\tau^- \rightarrow \nu_\tau + hadrons)$ in QCD. *Phys. Lett. B* **1991**, *259*, 144–150 [CrossRef]
16. Deur, A.; Brodsky, S.J.; de Téramond, G.F. Connecting the hadron mass scale to the fundamental mass scale of quantum chromodynamics. *Phys. Lett. B* **2015**, *750*, 528. [CrossRef]
17. Bjorken, J.D. Asymptotic Sum Rules at Infinite Momentum. *Phys. Rev.* **1969**, *179*, 1547–1553. [CrossRef]
18. Deur, A.; Brodsky, S.J.; de Téramond, G.F. The Spin Structure of the Nucleon. *Rep. Prog. Phys.* **2019**, *82*, 7. [CrossRef]
19. Kataev, A.L. The Ellis-Jaffe sum rule: The estimates of the next-to-next-to-leading order QCD corrections. *Phys. Rev. D* **1994**, *50*, 5469. [CrossRef]

20. Burkardt, M. Transverse force on quarks in deep-inelastic scattering. *Phys. Rev. D* **2013**, *88*, 114502. [CrossRef]
21. Deur, A. Spin Sum Rules and the Strong Coupling Constant at large distance. *AIP Conf. Proc.* **2009**, *1155*, 112–121.
22. Gerasimov, S.B. A Sum rule for magnetic moments and the damping of the nucleon magnetic moment in nuclei. *Sov. J. Nucl. Phys.* **1966**, *2*, 430.
23. Burkert, V.D. Comment on the generalized Gerasimov-Drell-Hearn sum rule in chiral perturbation theory. *Phys. Rev. D* **2001**, *63*, 097904. [CrossRef]
24. Brodsky, S.J.; de Téramond, G.F.; Deur, A. Nonperturbative QCD Coupling and its β-function from Light-Front Holography. *Phys. Rev. D* **2010**, *81*, 096010. [CrossRef]
25. Binosi, D.; Mezrag, C.; Papavassiliou, J.; Roberts, C.D.; Rodriguez-Quintero, J. Process-independent strong running coupling. *Phys. Rev. D* **2017**, *96*, 054026. [CrossRef]
26. Deur, A.; Burkert, V.; Chen, J.P.; Korsch, W. Experimental determination of the effective strong coupling constant. *Phys. Lett. B* **2007**, *650*, 244. [CrossRef]
27. Adeva, B.; Ahmad, S.; Arvidson, A.; Badelek, B.; Ballintijn, M.K.; Bardin, G.; Voss, R. Measurement of the spin dependent structure function g1(x) of the deuteron. *Phys. Lett. B* **1993**, *302*, 533. [CrossRef]
28. Airapetian, A.; Akopov, N.; Akushevich, I.; Amarian, M.; Arrington, J.; Aschenauer, E.C.; Schüler, K.P. The Q^2 dependence of the generalized Gerasimov-Drell-Hearn integral for the proton. *Phys. Lett. B* **2000**, *494*, 1–8. [CrossRef]
29. Deur, A.; Bosted, P.; Burkert, V.; Cates, G.; Chen, J.P.; Choi, S.; Yun, J. Experimental determination of the evolution of the Bjorken integral at low Q^2. *Phys. Rev. Lett.* **2004**, *93*, 212001. [CrossRef]
30. Anthony, P.L.; Arnold, R.G.; Band, H.R.; Borel, H.; Bosted, P.E.; Breton, V.; Zapalac, G. Deep inelastic scattering of polarized electrons by polarized He-3 and the study of the neutron spin structure. *Phys. Rev. D* **1996**, *54*, 6620. [CrossRef]
31. Alekseev, M.G.; Alexakhin, V.Y.; Alexandrov, Y.; Alexeev, G.D.; Amoroso, A.; Austregesilo, A.; Padee, A. The Spin-dependent Structure Function of the Proton g_1^p and a Test of the Bjorken Sum Rule. *Phys. Lett. B* **2010**, *690*, 466–472. [CrossRef]
32. Deur, A.; Prok, Y.; Burkert, V.; Crabb, D.; Girod, F.X.; Griffioen, K.A.; Kvaltine, N. High precision determination of the Q^2 evolution of the Bjorken Sum. *Phys. Rev. D* **2014**, *90*, 012009. [CrossRef]
33. Deur, A.; Chen, J.P.; Kuhn, S.E.; Peng, C.; Ripani, M.; Sulkosky, V.; Zheng, X. Experimental study of the behavior of the Bjorken sum at very low Q2. *Phys. Lett. B* **2022**, *825*, 136878. [CrossRef]
34. Rodríguez-Quintero, J.; Binosi, D.; Mezrag, C.; Papavassiliou, J.; Roberts, C.D. Process-independent effective coupling. From QCD Green's functions to phenomenology. *Few Body Syst.* **2018**, *59*, 121. [CrossRef]
35. Deur, A.; Shen, J.M.; Wu, X.G.; Brodsky, S.J.; de Téramond, G.F. Implications of the Principle of Maximum Conformality for the QCD Strong Coupling. *Phys. Lett. B* **2017**, *773*, 98. [CrossRef]
36. Deur, A.; Brodsky, S.J.; de Téramond, G.F. Determination of $\Lambda_{\bar{MS}}$ at five loops from holographic QCD. *J. Phys. G* **2017**, *44*, 105005. [CrossRef]
37. Cui, Z.F.; Ding, M.; Gao, F.; Raya, K.; Binosi, D.; Chang, L.; Roberts, C.D.; Rodríguez-Quintero, J.; Schmidt, S.M. Kaon and pion parton distributions. *Eur. Phys. J. C* **2020**, *80*, 1064. [CrossRef]
38. Janik, R.A. The Dynamics of Quark-Gluon Plasma and AdS/CFT. *Lect. Notes Phys.* **2011**, *828*, 147–181.
39. Busza, W.; Rajagopal, K.; van der Schee, W. Heavy Ion Collisions: The Big Picture, and the Big Questions. *Ann. Rev. Nucl. Part. Sci.* **2018**, *68*, 339–376. [CrossRef]
40. Florkowski, W.; Heller, M.P.; Spalinski, M. New theories of relativistic hydrodynamics in the LHC era. *Rept. Prog. Phys.* **2018**, *81*, 046001. [CrossRef]
41. Jokela, N.; Järvinen, M.; Remes, J. Holographic QCD in the Veneziano limit and neutron stars. *JHEP* **2019**, *3*, 41. [CrossRef]
42. Sulkosky, V.; Singh, J.T.; Peng, C.; Chen, J.P.; Deur, A.; Abrahamyan, S.; Zhu, L. Measurement of the ^3He spin-structure functions and of neutron (^3He) spin-dependent sum rules at $0.035 \leq Q^2 \leq 0.24$ GeV^2. *Phys. Lett. B* **2020**, *805*, 135428. [CrossRef]
43. Alcorn, J.; Anderson, B.D.; Aniol, K.A.; Annand, J.R.M.; Auerbach, L.; Arrington, J.; McKeown, R.D. Basic Instrumentation for Hall A at Jefferson Lab. *Nucl. Instrum. Meth. A* **2004**, *522*, 294–346. [CrossRef]
44. Mecking, B.A.; Adams, G.; Ahmad, S.; Anciant, E.; Anghinolfi, M.; Asavapibhop, B.; Vlassov, A.V. The CEBAF Large Acceptance Spectrometer (CLAS). *Nucl. Instrum. Meth. A* **2003**, *503*, 513–553. [CrossRef]
45. Prok, Y.; Bosted, P.; Kvaltine, N.; Adhikari, K. Precision measurements of g_1 of the proton and the deuteron with 6 GeV electrons. *Phys. Rev. C* **2014**, *90*, 025212. [CrossRef]
46. Zheng, X.; Deur, A.; Kang, H.; Kuhn, S.E.; Ripani, M.; Zhang, J.; Zachariou, N. Measurement of the proton spin structure at long distances. *Nat. Phys.* **2021**, *17*, 736. [CrossRef]
47. Adhikari, K.P.; Deur, A.; El Fassi, L.; Kang, H.; Kuhn, S.E.; Ripani, M.; CLAS Collaboration. Measurement of the Q2-dependence of the deuteron spin structure function g1 and its moments at low Q2 with CLAS. *Phys. Rev. Lett.* **2018**, *120*, 062501. [CrossRef]
48. Sulkosky, V. The Spin Structure of ^{3}He and the Neutron at Low Q^2: A Measurement of the Generalized Gdh Integrand. Ph.D. Thesis, College of William & Mary, Williamsburg, VA, USA, 2007.
49. Keith, C.D.; Anghinolfi, M.; Battaglieri, M.; Bosted, P.; Branford, D.; Bültmann, S.; Witherspoon, S. A polarized target for the CLAS detector. *Nucl. Instrum. Meth. A* **2003**, *501*, 327–339. [CrossRef]
50. Garibaldi, F.; Acha, A.; Ambrozewicz, P.; Aniol, K.A.; Baturin, P.; Benaoum, H.; Jefferson Lab Hall A Collaboration. High-resolution hypernuclear spectroscopy at Jefferson Lab, Hall A. *Phys. Rev. C* **2019**, *99*, 054309. [CrossRef]

51. Kim, J.H.; Harris, D.A.; Arroyo, C.G.; de Barbaro, L.; de Barbaro, P.; Bazarko, A.O.; Bernstein, R.H.; Bodek, A.; Bolton, T.; Budd, H.; et al. A measurement of $\alpha_s(Q^2)$ from the Gross–Llewellyn Smith sum rule. *Phys. Rev. Lett.* **1998**, *81*, 3595. [CrossRef]
52. De Alfaro, V.; Fubini, S.; Furlan, G. Conformal invariance in quantum mechanics. *Nuovo Cim. A* **1976**, *34*, 569. [CrossRef]
53. Trawinski, A.P.; Glazek, S.D.; Brodsky, S.J.; de Téramond, G.F.; Dosch, H.G. Effective confining potentials for QCD. *Phys. Rev. D* **2014**, *90*, 074017. [CrossRef]
54. Cornwall, J.M. Dynamical Mass Generation in Continuum QCD. *Phys. Rev. D* **1982**, *26*, 1453. [CrossRef]
55. Abbott, L.F. The Background Field Method Beyond One Loop. *Nucl. Phys. B* **1981**, *185*, 189–203. [CrossRef]
56. Binosi, D.; Chang, L.; Papavassiliou, J.; Roberts, C.D. Bridging a gap between continuum-QCD and ab initio predictions of hadron observables. *Phys. Lett. B* **2015**, *742*, 183–188. [CrossRef]
57. Aguilar, A.C.; Binosi, D.; Papavassiliou, J. Gluon and ghost propagators in the Landau gauge: Deriving lattice results from Schwinger-Dyson equations. *Phys. Rev. D* **2008**, *78*, 025010. [CrossRef]
58. Brodsky, S.J.; Shrock, R. Maximum wavelength of confined quarks and gluons and properties of quantum chromodynamics. *Phys. Lett. B* **2008**, *666*, 95. [CrossRef]
59. Sufian, R.S.; Liu, T.; de Téramond, G.F.; Dosch, H.G.; Brodsky, S.J.; Deur, A.; Hlfhs Collaboration. Nonperturbative strange-quark sea from lattice QCD, light-front holography, and meson-baryon fluctuation models. *Phys. Rev. D* **2018**, *98*, 114004. [CrossRef]